THE ASTROPHYSICAL JOURNAL, 327:248–264, 1988 April 1

PHOTOMETRIC AND SPECTROSCOPIC OBSERVATIONS OF THE ECLIPSING NOVA-LIKE VARIABLE PG 1030+590 (DW URSAE MAJORIS)

A. W. SHAFTER
McDonald Observatory and Department of Astronomy, University of Texas at Austin
F. V. HESSMAN
Max-Plank-Institut für Astronomie, Heidelberg
AND
E. H. ZHANG
Beijing Observatory, Academia Sinica, and Astronomy and Astrophysics Center, CCAST (World Laboratory)
Received 1987 June 30; accepted 1987 September 28

ABSTRACT

We present high-speed photometric and time-resolved spectroscopic observations of the nova-like variable PG 1030+590. The high-speed photometry revealed deep ($V \approx 1.5$ mag) eclipses which recur with a period of 0.13660653 (5) days. There is no evidence for a pronounced hump prior to eclipse although there is a suggestion of a broad hump, centered on eclipse, that shows up only in the ultraviolet. The eclipse profile is generally symmetric, but highly variable. The spectrum exhibits strong, high-excitation lines in the optical. Throughout most of the orbit He II λ4686 is stronger than Hβ, which is quite unusual except in highly magnetic systems. In addition the C III, N III complex at λ4640–4650 is present along with C II λ4267. These high-excitation lines are greatly diminished in intensity during eclipse. They arise in a relatively hot, localized region which we identify as the inner region of the accretion disk.

Radial velocity measurements show that the K-velocities of the Hα and Hβ emission lines are roughly 200 km s^{-1}. Such a high amplitude requires a white dwarf mass below 0.2 $M_\odot$ regardless of the orbital inclination or the evolutionary state of the secondary star. The K-velocity of the He II λ4686 line is considerably lower, about 110 km s^{-1}. We argue that the radial velocity variations of the He II emission better reflect the motion of the white dwarf because this line is formed near the center of the accretion disk close to the white dwarf. If we assume that $K_{\rm wd}$ is the same as the K-velocity of the He II λ4686 line and assume further that the secondary star is near the main sequence, we find $M_2 \approx 0.29\ M_\odot$, $M_1 \approx 0.9\ M_\odot$, and $i \approx 80°$. We stress that these values are subject to unknown and potentially large systematic errors. We conclude by discussing possible methods for improving determinations of $K_{\rm wd}$ for cataclysmic variables in general.

Subject headings: stars: dwarf novae — stars: eclipsing binaries — stars: individual (PG 1030+590) — stars: white dwarfs

I. INTRODUCTION

Cataclysmic variables are close binary systems consisting of a late-type, typically main-sequence star (the secondary) that fills its critical Roche surface and transfers material to a white dwarf companion (the primary). To conserve its angular momentum, the transferred material usually forms a ring or disk surrounding the white dwarf. A shock front or "hot spot" is formed near the outer rim where the interstar mass transfer stream impacts the disk. Comprehensive reviews of these systems can be found in Robinson (1976), Warner (1976), Cordova and Mason (1983), and Wade and Ward (1985).

Several years ago, Green, Ferguson, and Liebert (1982) published a list of cataclysmic variable candidates from the Palomar-Green survey for high-latitude, ultraviolet excess objects. As part of our general program of high-speed photometry of cataclysmic variables, we observed several objects on this list to search for eclipses or coherent periodicities in the light curves. These observations led to the discovery of eclipses in one of the objects, a $V = 14.5$ mag star, PG 1030+590 (Shafter and Hessman 1984).

The study of eclipsing cataclysmic variables can be fruitful. High-speed, multicolor photometry allows, among other things, the temperature distribution across the accretion disk to be determined (Zhang, Robinson, and Nather 1986; Horne 1985). In cases where the eclipse of the white dwarf and hot spot can be differentiated, high-speed photometric observations alone are sufficient to permit the masses and dimensions to be determined (see, e.g., Cook and Warner 1984). In other cases time-resolved spectroscopic data alone, or in conjunction with high-speed photometry, can be used to determine the masses and dimensions of the binary (see, e.g., Young, Schneider, and Shectman 1981; Kaitchuck, Honeycutt, and Schlegel 1983; Marsh, Horne, and Shipman 1987). With the intent of exploring the structure of PG 1030+590, we obtained high-speed photometry and extensive time-resolved spectroscopy of this system. We present the results of our photometric and spectroscopic studies of PG 1030+590 in this paper.

II. PHOTOMETRY

a) Observations

The photometric observations of PG 1030+590 were obtained with a two-star, high-speed photometer mounted at the Cassegrain focus of the McDonald Observatory 2.1 m reflector. A complete description of the photometer can be found in Nather (1973). The data were acquired on several observing runs between 1983 December and 1986 December. Some of these observations were obtained through Johnson

TABLE 1

SUMMARY OF PHOTOMETRIC OBSERVATIONS

HJD (2,440,000+)	Telescope	Int. Time (s)	Duration (hr)	Filters
5683.9387 (1983 Dec 15)	2.1 m	1	2.0	None
5685.7848 (1983 Dec 17)	0.9 m	3	5.6	None
5800.7807 (1984 Apr 10)	2.1 m	1	2.8	*U*, *B*, *V*
5801.8208 (1984 Apr 11)	2.1 m	1	1.0	*U*, *B*, *V*
5802.6053 (1984 Apr 12)	2.1 m	1	3.5	*U*, *B*, *V*
5802.7682 (1984 Apr 12)	2.1 m	1	1.1	*U*, *B*, *V*
6106.9583 (1985 Feb 10)	2.7 m	5	1.4	None
6173.6279 (1985 Apr 18)	2.1 m	3	1.9	*B*, *V*, *R*
6388.9565 (1985 Nov 19)	2.1 m	3	0.8	None
6773.8420 (1986 Dec 9)	2.1 m	2	3.8	None

UBV filters, some with *BVR* filters, and the rest in "white" light (no filters). The bandpass of the filterless data was determined by the response of the RCA 8850 tube used in the primary channel. The response of this tube results in an effective wavelength similar to that of the Johnson *B* filter, but the bandpass is much wider. The *UBV* data were also obtained with the RCA 8850 tube, but the *BVR* data were acquired with an extended red RCA 9658 tube. A summary of our photometric observations is presented in Table 1.

The data were reduced by subtracting the contribution due to sky background and dark noise and then correcting for the effects of atmospheric extinction using mean extinction coefficients for McDonald Observatory. The filter photometry was calibrated by observing a nearby comparison star ~ 6 minutes north of PG 1030+590. We calibrated the *B*, *V*, and *R* magnitudes of the comparison star using standards from Moffat and Barnes (1979).

Figures 1 and 2 show light curves covering two eclipses of PG 1030+590. The light curves in Figure 1 were obtained on 1984 April 10. We used an integration time of 1 s per filter and since the photometer cycles successively through the filters, the time resolution is 3 s. The light curve shown in Figure 2 was obtained 1 yr later, this time using *B*, *V*, and *R* filters. The integration time for these data was 3 s per filter resulting in an overall time resolution of 9 s.

We observed a total of 10 eclipses of PG 1030+590. The times of mid-eclipse, which were determined in a manner similar to that employed by Zhang, Robinson, and Nather (1986) in their analysis of HT Cas, are presented in Table 2. A linear least-squares fit to the eclipse timings yields the following ephemeris for the time of mid-eclipse:

$$T_{\rm eclipse} = \text{HJD } \underset{(15)}{2446229.00704} + \underset{(5)}{0.1660653}E$$

The differences between the observed and calculated times of mid-eclipse are given in Table 2 and plotted as a function of cycle number in Figure 3. As expected, there is no evidence for a change in the orbital period over the 3 yr baseline of available eclipse timings.

b) *Light Curve Morphology*

There are several distinguishing characteristics of the light curve of PG 1030+590. Perhaps the most obvious is the absence of a general increase in brightness or "hump" just prior to eclipse. In those systems in which an orbital hump is observed, the hump is usually explained as a result of the varying aspect of a bright spot on the outer rim of the accretion disk. The bright spot in turn is believed to be caused by the impact of the interstar mass transfer stream (Smak 1971). The overwhelming majority of systems which show large pre-eclipse humps in their light curves are dwarf novae. Typical examples are U Gem (Warner and Nather 1971), and Z Cha (Wood *et al.* 1986, and references therein).

The fact that most quiescent dwarf novae are observed to have more conspicuous hot spots than nova-like variables strongly suggests that steady accretion (mass transfer rate = mass accretion rate) does not usually occur in quiescent dwarf novae. To first order, the hot spot luminosity is proportional to the mass *transfer* rate from the secondary star, while the disk luminosity is proportional to the mass *accretion* rate through the disk. Consequently, if we assume steady accretion, then the ratio of hot spot to disk luminosity should be essentially independent of the mass transfer rate (i.e., independent of whether the system is a dwarf nova or a nova-like variable). The fact that the ratio of hot spot to disk luminosity in quiescent dwarf novae is typically *higher* than it is in nova-like variables (or in outbursting dwarf novae) would appear to provide additional support for theories of dwarf nova eruptions invoking nonsteady accretion, such as the disk instability theories (Smak 1984; Shafter, Wheeler, and Cannizzo 1986 and references therein).

Although the eclipses displayed in Figures 1 and 2 are alike in the sense that they do not show bright spots, their overall shape is different. The eclipses shown in Figure 2 are smooth and rounded while those shown in Figure 1 have a complex structure. The structure of the accretion disk in PG 1030+590 must be quite variable. We will defer a fuller discussion of the light curve morphology to a subsequent paper (Shafter, Wood, and Robinson 1988; Paper II).

III. SPECTROSCOPY

a) *Observations*

Our spectroscopic observations of PG 1030+590 were obtained using two different instruments on two different telescopes. One set of observations were obtained with a CCD spectrograph at the Cassegrain focus of the McDonald 2.1 m reflector and the other set with an image dissector scanner (Robinson and Wampler 1972) at the Cassegrain focus of the Mount Lemmon Observatory 1.5 m reflector. We acquired the McDonald observations during four nights in 1984 March. The Mount Lemmon data were obtained a few weeks later in

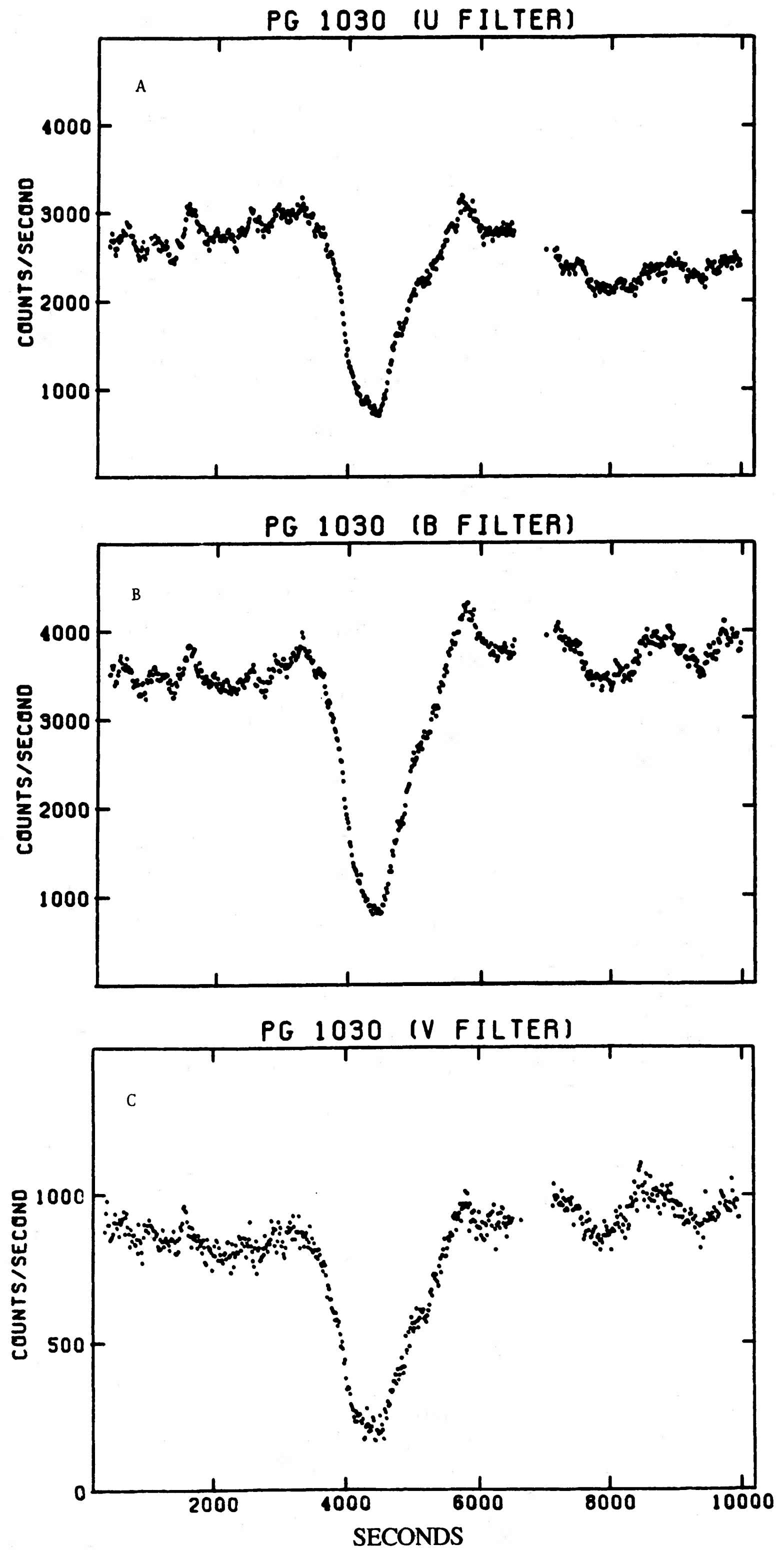

FIG. 1.—*UBV* light curves of PG 1030+590 obtained on 1984 April 10. There is no evidence for a pre-eclipse brightening or "hump" prior to eclipse as usually observed in dwarf novae. The *U* band light curve does however show evidence for a broad hump centered on eclipse.

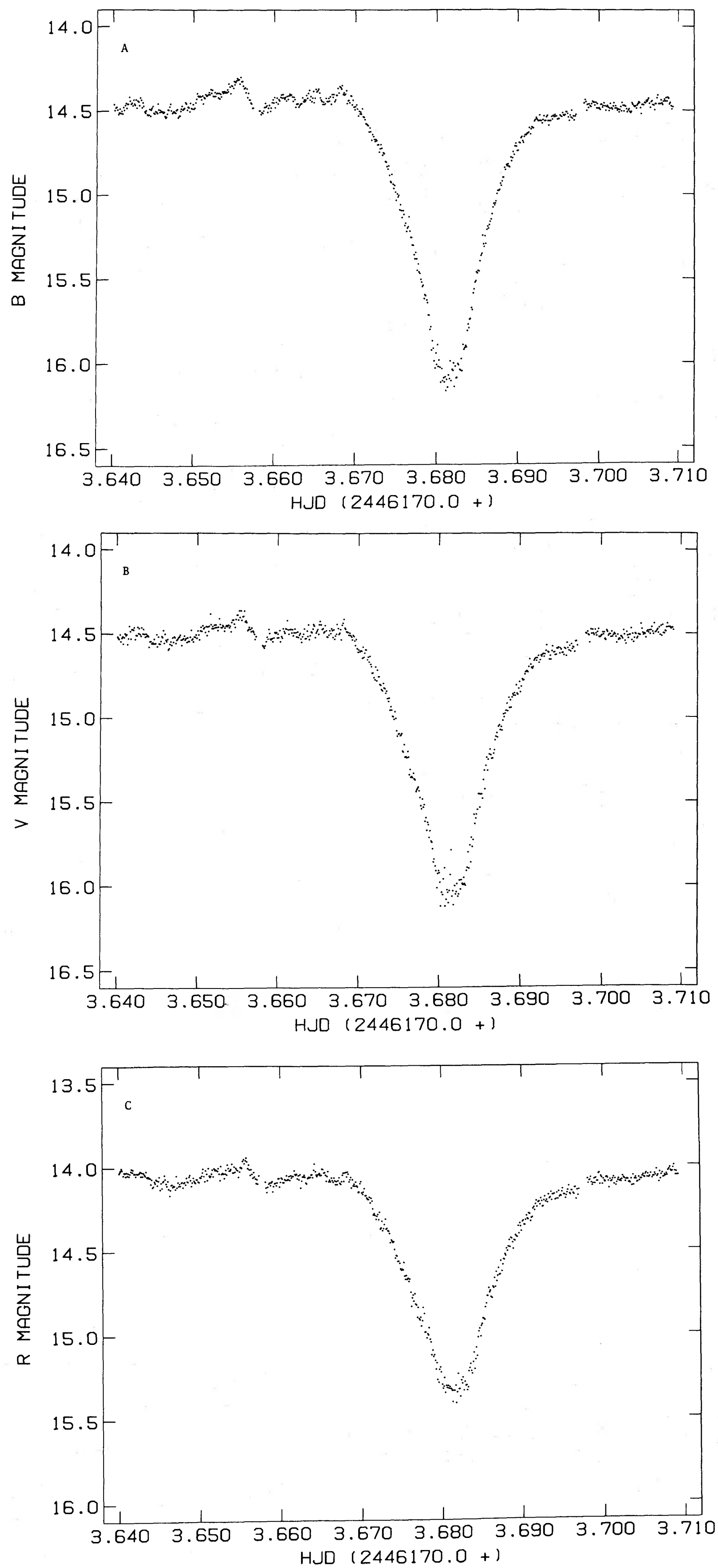

FIG. 2.—*BVR* light curves obtained on 1985 April 18. Again there is no evidence for a hump in the light curve prior to eclipse. The eclipse depth increases with decreasing wavelength. Note the smooth rounded eclipse profile unlike the more complicated eclipse morphology displayed in Fig. 1.

TABLE 2

ECLIPSE OBSERVATIONS OF PG 1030+590

HJD (mid-eclipse) (2,440,000+)	Cycle Number (N)	$O-C$[a] (cycles)
5683.9467 (1983 Dec 15)	−3990	−0.0020
5685.9967 (1983 Dec 17)	−3975	0.0046
5800.8822 (1984 Apr 10)	−3134	0.0002
5801.8385 (1984 Apr 11)	−3127	0.0006
5802.6577 (1984 Apr 12)	−3121	−0.0026
5802.7948 (1984 Apr 12)	−3120	0.0010
6107.0169 (1985 Feb 10)	−983	−0.0037
6173.6817 (1985 Apr 18)	−405	0.0023
6388.9729 (1985 Nov 19)	1171	−0.0028
6773.9308 (1986 Dec 9)	3989	0.0023

[a] Calculated times of mid-eclipse based on linear ephemeris given in text.

1984 and again in 1985 February. The details of the spectroscopic observations are summarized in Table 3.

The McDonald observations were obtained using an RCA CCD. A 1200 line mm^{-1} grating was used in first order and resulted in a reciprocal dispersion of approximately 1.75 Å channel^{-1}. The slit width was set by the seeing. A typical width of order of 2″ yielded a spectral resolution of ~3 Å FWHM. The CCD was oriented so that the dispersion was along the long axis of the chip (512 elements). This configuration resulted in a wavelength coverage of ~900 Å. We centered the spectrum at roughly 4600 Å so that we covered Hγ, Hβ, and the He II λ4686 emission features.

The Mount Lemmon observations include both low- and high-resolution spectra. The low-resolution data were obtained during the 1984 run and consist of a 1 hr sequence of 1 minute spectra centered on eclipse. Our purpose in acquiring these data was to study the spectral changes in and out of eclipse. These observations were obtained by using a 600 line mm^{-1} grating in first order and cover ~3800–7000 Å. A relatively large 6″.5 circular aperture was used in order to minimize slit losses. The absolute fluxes have been calibrated by comparison with standard stars observed by Stone (1977). The weather was clear and we expect that the absolute fluxes should be accurate to a few percent. The higher resolution observations were obtained by using a 1200 line mm^{-1} grating in first order. These data cover roughly 5800–7000 Å at a resolution of ~4 Å FWHM. A smaller 3″.1 aperture was used to improve the spectral resolution. Absolute fluxes were not required in this case because these data were obtained for use in the radial velocity study. A discussion of the spectral stability of the Mount Lemmon IDS and a further description of our observing technique can be found in Shafter and Harkness (1986).

Our low-resolution IDS spectra are displayed in Figure 4. We have summed the 57 individual 1 minute spectra into two bins—one in and one out of eclipse. The in-eclipse bin contains 15 spectra centered on mid-eclipse. The other spectrum is composed of a sum of all the remaining spectra. Table 4 gives the equivalent widths and fluxes of the stronger emission lines in the two summed spectra. Two general observations can be made from an inspection of Figure 4 and Table 4. First, with the exception of the high-excitation emission lines (C II λ4267, C III λ4640, and He II λ4686), the equivalent widths of the lines increase significantly during eclipse while the line fluxes stay approximately constant (slightly decreasing during eclipse). Essentially the opposite occurs in the case of the low-excitation lines. This behavior can be seen clearly by comparing the strength of He II λ4686 with Hβ for the two spectra shown in Figure 4.

It is clear that the eclipsed region contributes significantly to the continuum emission, and it contributes significantly to the formation of the high-excitation emission lines, but it contributes little to the low-excitation Balmer and He I emission. The eclipsed region is therefore relatively hot and is likely to be either the inner region of the accretion disk or the hot spot. We

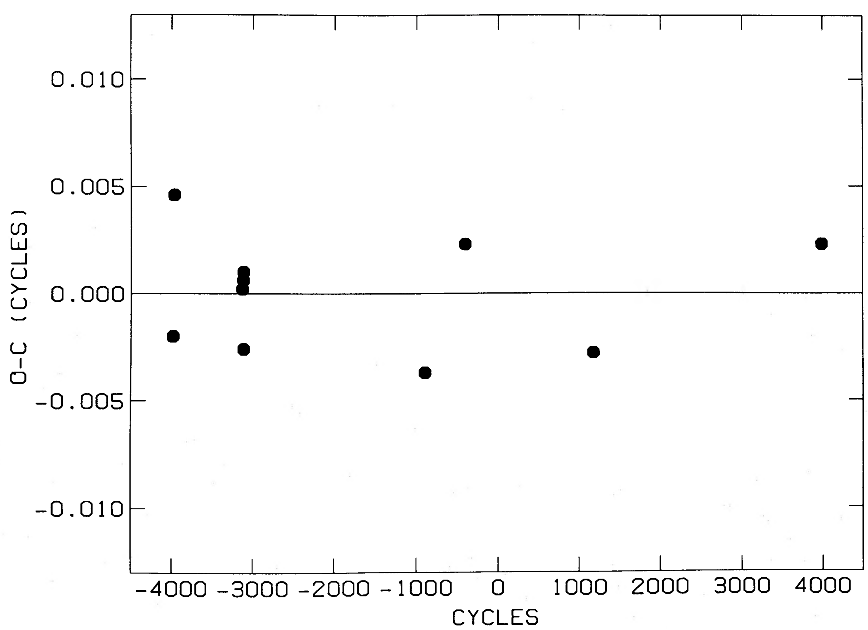

FIG. 3.—The $O-C$ diagram for the orbital period of PG 1030+590. The phase difference between the observed times of mid-eclipse and the predicted times of mid-eclipse as calculated from the best linear ephemeris are plotted as a function of the orbital cycle number. The observed scatter is consistent with measurement error. As expected, there is no evidence for a change in the orbital period.

TABLE 3

SUMMARY OF SPECTROSCOPIC OBSERVATIONS

HJD (2,440,000+)	Telescope	Int. Time (minutes)	Duration (hr)	Coverage (λ)	Resolution (Å)
5768.665 (1984 Mar 9)	McDonald 2.1 m	5	5.5	4200–5100	3
5769.649 (1984 Mar 10)	McDonald 2.1 m	5	7.0	4200–5100	3
5770.645 (1984 Mar 11)	McDonald 2.1 m	5	7.5	4200–5100	3
5771.638 (1984 Mar 12)	McDonald 2.1 m	5	7.5	4200–5100	3
5791.845 (1984 Apr 1)	Mt. Lemmon 1.5 m	1	1.0	3800–7000	11
5792.676 (1984 Apr 02)	Mt. Lemmon 1.5 m	4	3.5	5800–7000	4
6116.860 (1985 Feb 20)	Mt. Lemmon 1.5 m	4	3.0	5800–7000	4

have already seen from the eclipse morphology that the hot spot does not appear to be a significant source of continuum emission in PG 1030+590. It is therefore likely that high-excitation emission arises in or just above the inner part of the disk. This conclusion has also been reached by Honeycutt, Schlegel, and Kaitchuck (1986) in their study of a similar system, PG 1012−035 (SW Sex). The lower excitation lines are probably formed in the outer regions of the disk or in a corona above the disk.

There are two additional spectral characteristics which should be pointed out. First, there is no evidence for Fe II emission at λ5169. Consequently, the He I emission at λ4921 and λ5015 is probably not blended with Fe II λ4923 and λ5018 emission. The Fe II lines are usually seen in low-excitation systems, such as dwarf novae, which also exhibit strong He I emission. Second, the out-of-eclipse spectrum exhibits C II λ4267 emission. This line has a relatively high excitation temperature and is usually observed only in the magnetic systems (AM Her and DQ Her systems). In these systems the accretion is funneled onto a relatively small region of the white dwarf causing the temperature of this region to be high.

IV. RADIAL VELOCITIES

The emission lines observed in cataclysmic variables typically have a complex structure, with separate components which can arise from the hot spot (Stover 1981), the secondary star (Schneider, Young, and Shectman 1981; Shafter *et al.* 1985; Hessman 1986), or from unexpected regions of the disk (Shafter, Szkody, and Thorstensen 1986; Kaitchuck, Honeycutt, and Schlegel 1983; Gilliland, Kemper, and Suntzeff 1986). These components are known to distort the radial velocity curves of the white dwarfs, but the extent of the distortion is unknown. The usual practice of measuring the wings of the emission lines, which are predominantly formed in the inner regions of the accretion disk, is believed to minimize this distortion, but unknown and potentially large systematic effects are still thought to be present.

To study the emission line structure in PG 1030+590, we have followed the procedure outlined in Shafter (1985), and Shafter, Szkody, and Thorstensen (1986). Specifically, we have measured radial velocities of the Hα, Hβ, and the He II λ4686 by convolving the data with a template consisting of two

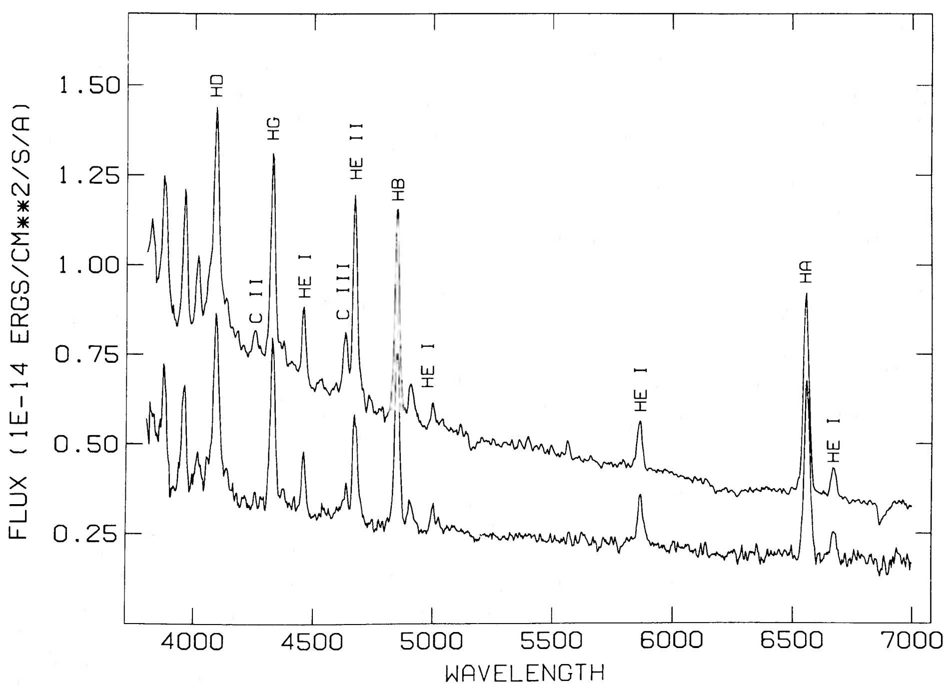

FIG. 4.—The low-resolution Mount Lemmon spectra. The absolute flux (ergs cm^2 s^{-1} Å^{-1}) of PG 1030+590 both in and out of eclipse is plotted as a function of wavelength. Note the reduction in the flux of He II λ4686 and C II λ4267 during eclipse.

TABLE 4

EQUIVALENT WIDTHS AND LINE FLUXES OF PRINCIPLE OPTICAL EMISSION LINES[a]

Line	Equivalent Width (Å)	Flux (10^{-14} ergs cm^{-2} s^{-1} $Å^{-1}$)
He I λ4026	5 (9)	4.13 (3.30)
Hδ	26 (54)	21.8 (19.2)
C II λ4267	2 (−)	1.57 (−)
Hγ	18 (36)	13.4 (12.2)
He I λ4471	6 (10)	3.79 (3.23)
C III, N III λ4645	7 (9)	4.25 (2.72)
He II λ4686	22 (28)	13.9 (7.91)
Hβ	26 (46)	14.9 (12.4)
He I λ4922	5 (8)	2.70 (2.13)
He I λ5015	− (7)	− (1.85)
He I λ5876	8 (23)	3.57 (4.98)
Hα	45 (77)	16.3 (14.2)
He I λ6678	6 (11)	2.16 (2.00)

[a] Values in parentheses are in eclipse.

narrow Gaussians, one in the red wing of the line and the other in the blue wing. The position at which the intensities through the two Gaussians become equal is a measure of the wavelength of the emission line (Schneider and Young 1980). By varying the separation between the two Gaussians the orbital phase dependent structure of the emission lines may be studied.

Because of the relatively large number of CCD spectra, we have co-added the individual spectra into 20 orbital phase bins prior to measuring the velocities. We have relatively few IDS spectra, on the other hand, so these spectra have been measured individually. In previous analyses (e.g., Shafter, Szkody, and Thorstensen 1986), we parameterized the Gaussian separation with the parameter, *a*, which was equal to the half-separation of the Gaussian bandpasses. Here we will refer to the full Gaussian separation, *s*. In addition, because we are dealing with several spectral lines instead on just one as in past analyses, we parameterize *s* in terms of velocity rather than wavelength.

For measurements made with a given value of *s*, we have made a nonlinear least-squares fit of the resulting velocities to sinusoids of the form

$$V(t, s) = \gamma(s) + K_{\rm em}(s) \sin \{2\pi[t - t_0(s)]/P\} ,$$

where P is the orbital period determined in § II. We have fitted the velocities for the three emission lines separately in order to test for consistency in the derived radial velocity amplitudes and in the times of spectroscopic conjunction ($t_0[s]$) relative to the time of mid-eclipse (T_0).

To help assess the reliability of the derived orbital elements it is instructive to plot $K_{\rm em}$, its associated error σ_K/K, γ, and $\Delta\phi$ ($=[t_0(s) - T_0]/P$) as functions of *s*. The resulting plot or "diagnostic diagram" reveals the degree of orbital phase dependent asymmetry in the emission line profile as a function of velocity from line center (i.e., as a function of *s*). If the hot spot emission is confined to the outer regions of the accretion disk where the Keplerian velocities are low, we would expect the disk emission to become axisymmetric in the high-velocity line wings. The orbital elements should then converge to their true values for sufficiently large values of the Gaussian separation, *s* (for a more extensive discussion of the diagnostic diagram and its interpretation refer to Shafter, Szkody, and Thorstensen [1986]).

The diagnostic diagrams based on the Hα, Hβ, and He II λ4686 lines are shown in Figures 5–8. We begin by discussing the diagnostic diagrams for the Hα data. Although the orbital period is known accurately enough to phase our two Mount Lemmon runs together we decided to analyze the data sets separately. In this way we are able to check for constancy in the orbital solutions. Agreement between the two epochs would suggest that PG 1030+590 was not in an unusual state during our observations. The diagnostic diagram based on our 1984 April Mount Lemmon run is presented in Figure 5. In keeping with the usual philosophy that one should measure as far out in the line wings as is practicable, the preferred value of K_1 is found at a separation of 1800 km s^{-1}. At larger separations, the velocity measurements become less reliable because the Gaussians are no longer sampling a significant portion of the emission line wings. This point is indicated by the abrupt increase in σ_k/K. Regardless of the Gaussian separation, the *K*-velocity is always greater than $\sim$230 km s^{-1}! This is a distressing result. It is not difficult to show that such a high value of $K_{\rm wd}$ requires the mass of the white dwarf to be extremely low. Even if we take the worst case and assume that the secondary is on the main sequence and the orbital inclination is 90° (so that the orbital velocity is equal to, but not greater than, $K_{\rm em}$), we find that the mass of the white dwarf must be less than 0.18 $M_\odot$ for $K_{\rm wd} > 230$ km s^{-1}; this seems unlikely. If the secondary is out of thermal equilibrium as a result of rapid mass loss, a situation which is expected for systems just above the period gap (Rappaport, Verbunt, and Joss 1983), the secondary star will be too large for its mass, the white dwarf will have a correspondingly lower mass, and the problem is exacerbated.

Before leaving our discussion of Figure 5, we wish to comment on the observed phase shift between spectroscopic conjunction (superior conjunction of the emission line source—presumably the disk and white dwarf) and photometric conjunction (mid-eclipse). We have defined the phase shift to be positive if the spectroscopic conjunction occurs *after* photometric conjunction (i.e., $\Delta\phi = 360\ [t_0 - T_0]/P$ deg). In the absence of nonaxisymmetric disk emission components, such as hot spot emission, we would expect the phase shift to be zero. On the other hand, if emission from the hot spot is affecting the velocity measurements, and if the hot spot is located on the trailing side of the disk as expected, then we would expect a positive phase shift. Referring to Figure 5, we see that this is indeed the case.

The results from our Mount Lemmon run from 1985 February are displayed in Figure 6. These data confirm the high *K*-velocity and the sign of the phase shift observed nearly a year earlier. The amplitude is somewhat smaller but is usually in excess of 200 km s^{-1}. The most likely value is near 220 km s^{-1}. The phase shift is somewhat larger than in the 1984 April data but is consistent with that expected from hot spot contamination.

Figure 7 shows the diagnostic diagram for the Hβ emission line. The radial velocity amplitude increases steadily as the Gaussian separation is increased. Beyond a separation of 2400 km s^{-1} the amplitude begins to level off at a value of $\sim$190 km s^{-1}. This amplitude is in reasonable agreement with, albeit somewhat smaller than, the values derived from the Mount Lemmon Hα data. Although, for the reasons described earlier, a lower value of $K_{\rm wd}$ is more in line with what we would expect for a system with a period of $\sim$3 hr, values of $\sim$190 km s^{-1} still result in an uncomfortably low white dwarf mass.

The primary result of the Balmer line analysis is that the emission line amplitudes appear to be quite large, implying a

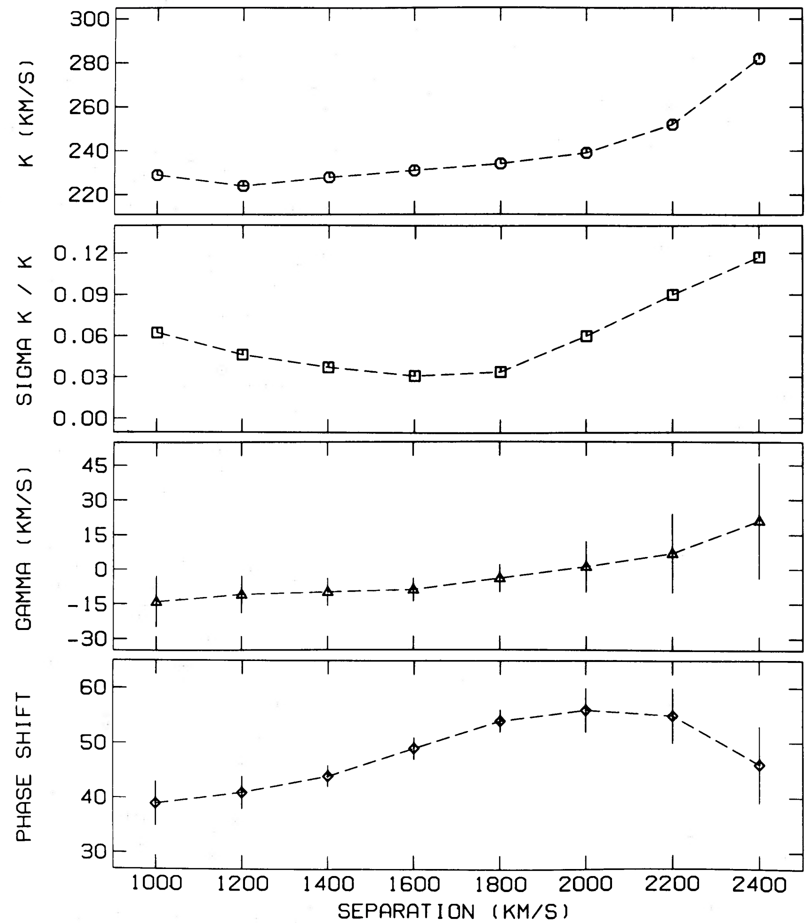

FIG. 5

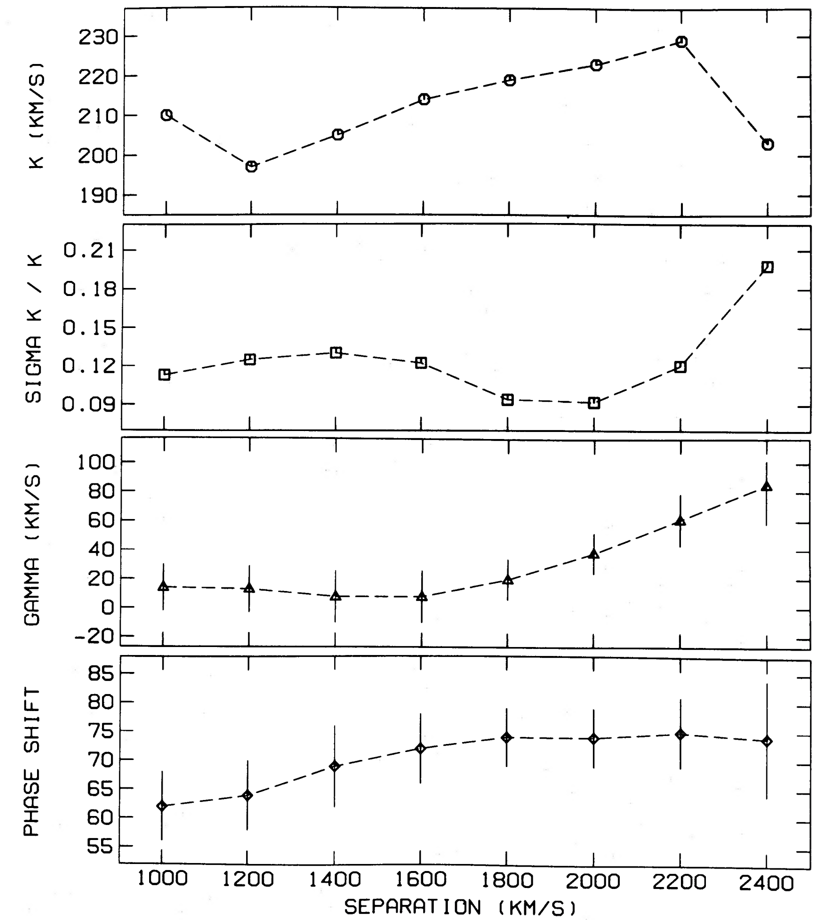

FIG. 6

FIG. 5.—The diagnostic diagram based on the 1984 April 2 Mount Lemmon Hα observations. It is clear that for any reasonable value of the Gaussian separation the measured radial velocity amplitude is in excess of 220 km s^{-1}. The Hα lines can be measured out to $\sim$900 km s^{-1} (a Gaussian separation of 1800 km s^{-1} before the measurements become noisy. Note that the phase shift between the time of spectroscopic conjunction and the time of mid-eclipse *increases* as a function of the Gaussian separation. This behavior is not expected if the phase shift were caused by hot-spot emission which is confined to the outer region of the disk where the Keplerian velocities are relatively low.

FIG. 6.—The diagnostic diagram based on the 1985 February 25 Mount Lemmon Hα observations. As was the case for the 1984 April data (Fig. 5) the measured radial velocity amplitude is generally in excess of 200 km s^{-1}. The Gaussian separation may be increased to a value of near 2200 km s^{-1} before the line flux becomes too weak to allow reliable velocity measurements. At a separation of 2200 km s^{-1} the K-velocity is about 220 km s^{-1} in good agreement with the amplitude measured from the 1984 April data. Once again the phase shift seems to increase as a function of the Gaussian separation.

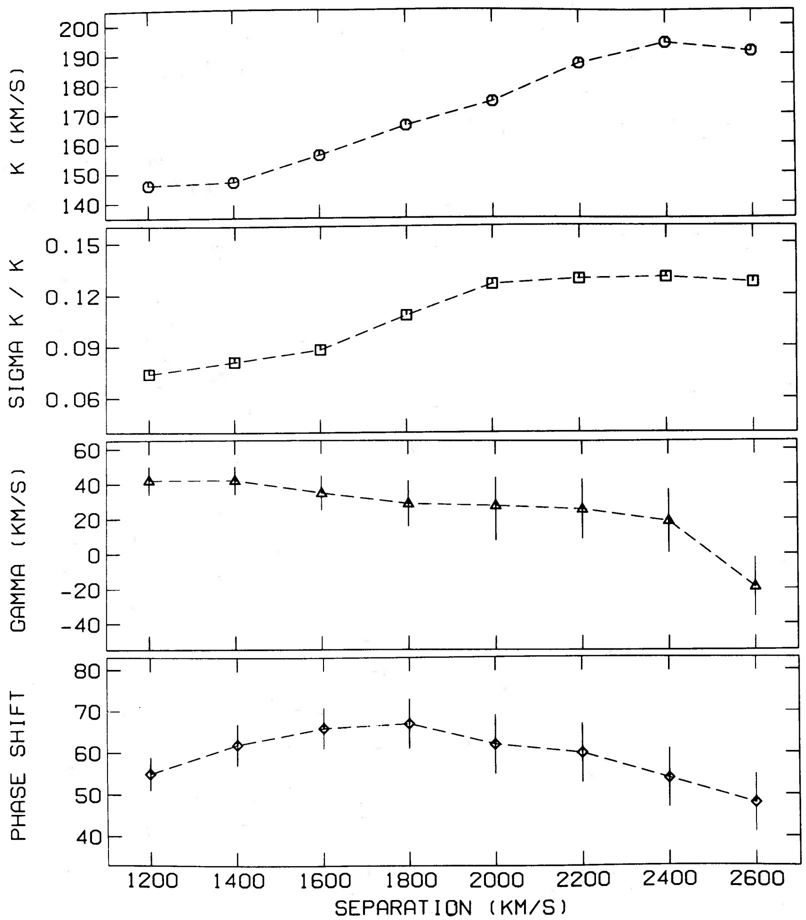

FIG. 7

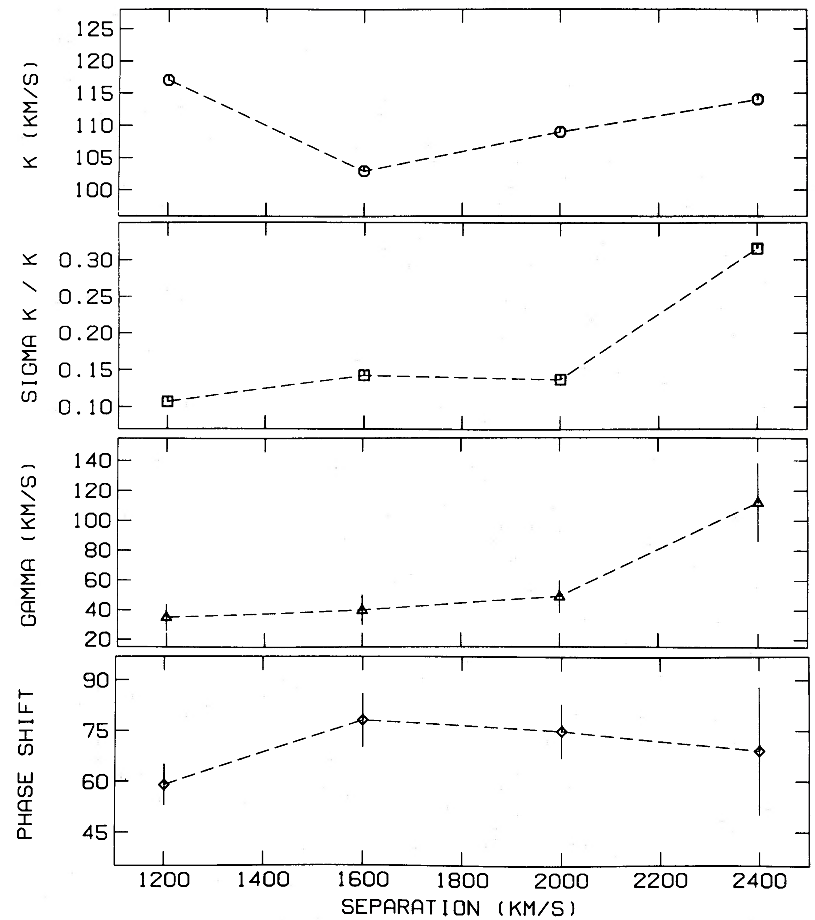

FIG. 8

FIG. 7.—The diagnostic diagram based on the 1984 March McDonald Hβ observations. The velocity amplitude derived from the Hβ data increases with increasing Gaussian separation. Generally the amplitude is smaller than that derived from the Mount Lemmon Hα observations; however, for relatively large Gaussian separations the K-velocity is not inconsistent with the results of the Hα observations. Unlike the Hα observations the phase shift is a roughly constant function of the Gaussian separation.

FIG. 8.—The diagnostic diagram based on the 1984 March McDonald He II λ4686 observations. Measurements of the He II emission lines yield K-velocities which are significantly smaller than those derived from the Balmer lines. The Gaussian separation may be increased to $\sim$2000 km s^{-1} before the measurements become noisy. At a separation of 2000 km s^{-1} the K-velocity is $\sim$109 km s^{-1}. This value is more likely to represent the K-velocity of the white dwarf than the values derived from the Balmer lines. It is unclear, however, why the phase shift should be so large if the He II emission is not strongly affected by the hot spot.

TABLE 5

ORBITAL PARAMETERS

Date	Line	Gaussian Sep. (km s^{-1})	K_{em} (km s^{-1})	γ (km s^{-1})	$\Delta\phi$ (deg)
1984 Apr	Hα	1800	234(8)	14(6)	54(2)
1985 Feb	Hα	2000	223(21)	45(14)	74(5)
1984 Mar	Hβ	2400	194(25)	19(18)	54(7)
1984 Mar	He II λ4686	2000	109(15)	49(11)	75(8)

low mass for the white dwarf if accepted at face value, and the phase shift between spectroscopic conjunction and mid-eclipse for both Hα and Hβ is significant. Both the high amplitude and the phase shift can be qualitatively explained if we invoke contamination of the disk profile by hot spot emission. A bright spot on the trailing side of the disk is expected to delay the time of spectroscopic conjunction, as observed. In addition, if the contamination is sufficiently extensive, the measured radial velocity amplitude may be increased because the Keplerian velocity at the outer edge of the accretion disk is typically larger than the orbital velocity of the white dwarf. It is somewhat surprising, however, that the amplitude and the phase shift do not decrease with increasing Gaussian separation; instead they both appear to increase. Clearly, this is not the behavior expected if the hot spot is confined to a localized region near the perimeter of the disk. *We speculate that the hot spot (or at least a region of enhanced line emission) extends far into the disk and is capable of affecting the velocity measurements at large distances from line center.*

Fortunately we have radial velocity information from He II λ4686 as well as from the Balmer lines. Such data are valuable because the He II line has a much higher excitation temperature than the Balmer lines and is therefore expected to form in a different (hotter) and more localized region of the accretion disk. There are two plausible locations for the origin of the He II emission: (1) in or above the central regions of the accretion disk, or (2) near the hot spot. Although the time resolution of our spectrophotometry during eclipse is insufficient to establish conclusively that the eclipse of the He II emission is centered on the broad-band eclipse, a visual examination of Figure 16 of Honeycutt, Kaitchuck, and Schlegel (1987) indicates that the He II λ4684 emission is eclipsed near orbital phase 0. Furthermore, studies of similar systems have shown that the He II emission is eclipsed simultaneously with the continuum eclipse (Honeycutt, Schlegel, and Kaitchuck 1986; Penning *et al.* 1983; Downes *et al.* 1986). This result strongly suggests that the He II emission arises in or near the inner regions of the accretion disk. In addition s-wave components, which are normally associated with hot spot emission, are not observed in He II emission. In view of this evidence, we feel confident that the He II emission is produced primarily in the inner disk region. As a result, we expect that the radial velocity variations of the He II emission will reflect the motion of the white dwarf with more reliability than will the Balmer emission.

Figure 8 shows the results of our analysis of the He II emission line. We have been unable to measure the velocities out to large distances from line center because of the presence of the C III feature at λ4650. Nevertheless, it is clear that the value of K_{em} is significantly smaller than the values based on the Balmer lines and is closer to the velocity expected for a typical white dwarf mass. The phase shift initially increases with Gaussian separation as does the phase shift determined from the Balmer lines, but then starts to gradually decrease, as expected, for separations larger than 1600 km s^{-1}. Since the He II emission is produced primarily in the inner disk region, it is not clear why the observed phase shift of the Balmer emission should be so large. It appears that either some fraction of the He II emission is produced in the vicinity of the hot spot or that, as we suspected in the case of the Hα emission, the hot spot is strongly disturbing the inner disk. Consequently, even the He II radial velocity amplitude cannot be viewed as reliable.

The best-fit values for the orbital elements $\gamma(s)$, $K_{em}(s)$, and $t_0(s)$ for the Hα, Hβ, and the He II λ4686 lines are presented in Table 5. In each case the final orbital elements are based on velocity measurements made using the preferred value of the Gaussian separation as suggested from the diagnostic diagrams. Specifically, we used separations of 1800, 2000, 2400, and 2000 km s^{-1} for the 1984 April Hα, the 1985 February Hα, the Hβ, and the He II data, respectively. In all cases we employed Gaussian widths of 300 km s^{-1} FWHM.

The radial velocity curves based on each of the 4 data sets are shown in Figures 9–12. In each case we have folded the individual velocity measurements with the orbital period and plotted them as a function of the *photometric* phase. (A photometric phase of 0.0 corresponds to mid-eclipse.) In the case of the Mount Lemmon Hα data, the observations for each year were obtained on a single night and span slightly more than one orbital period. Thus individual points in the radial velocity curves represent single 16 minute integrations. As described earlier, due to the large number of individual spectra, the CCD data, which cover both Hβ and He II λ4686, have been folded with the orbital period and co-added into 20 phase bins prior to measurement. Consequently, the radial velocity curves display the velocities derived from the 20 phase-binned spectra, not individual spectra. Again the velocities are plotted as a function of photometric phase.

Figure 13 illustrates our phase-binned CCD spectra. For clarity we have reduced the total number of phase bins from the 20 used in the radial velocity study to 10. He II λ4686 is stronger than Hβ at all orbital phases except near eclipse. Perhaps more interestingly, however, the Balmer and He I lines become clearly doubled between orbital phases 0.4 and 0.6, when the disk is at inferior conjunction. An expanded view of the spectral region near Hβ is shown in Figure 14. The observed line doubling near orbital phase 0.5 has been seen in other eclipsing cataclysmic variables (e.g., PG 1012−035, Honeycutt, Schlegel, and Kaitchuck (1986); V1315 Aql, Downes *et al.* 1986). Honeycutt, Schlegel, and Kaitchuck (1986) have suggested that the absorption near phase 0.5 may be caused by absorption by material ejected from the system through the outer Lagrangian point. Downes *et al.* suggested independently that this effect may be causing the line doubling observed in V1315 Aql. They went on to speculate that the fact

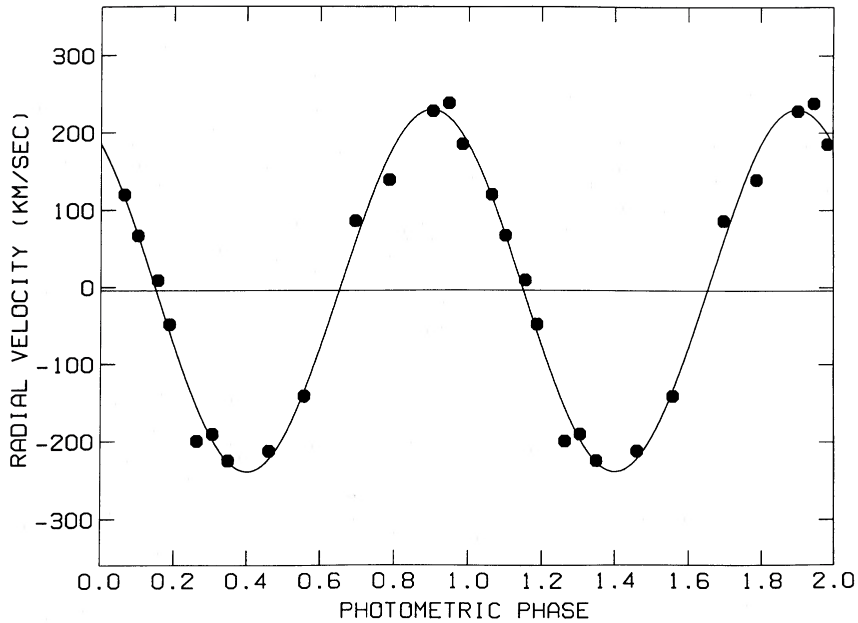

FIG. 9.—The radial velocity curve for the 1984 April 2 Mount Lemmon Hα observations. The data are folded with the orbital period and plotted as a function of orbital phase. The measurements were made using a Gaussian width of 300 km s^{-1} and a separation of 1800 km s^{-1}. The amplitude is 234 km s^{-1}.

that the mass transfer stream is occulted near phase 0.5 may provide a possible clue to the nature of the absorption. If the hot spot and the mass transfer stream, or both, contribute significantly to the low-excitation Balmer and He I line emission then this emission may fill in the normally double-peaked disk profile at orbital phases where the stream is not occulted.

Although both effects may be contributing to the observed absorption in PG 1030+590 and similar systems, we marginally favor the second interpretation. We have already presented evidence that an additional source of Balmer (and possibly He I) line emission is contaminating the emission line profiles in PG 1030+590, and this emission may be sufficient to fill in the disk emission profile. If this excess emission arises in the vicinity of the hot spot or stream as we suspect, then the occultation of this region at phase 0.5 seems sufficient to explain the double-peaked structure seen at this phase. Thus there may be no need to invoke additional absorption by material near the outer Lagrangian point although such material may exist. A potential problem with this interpretation concerns the fact that the lines are not observed to be doubled during primary eclipse. In particular, if occultation of the stream and hot spot emission by the disk is invoked to

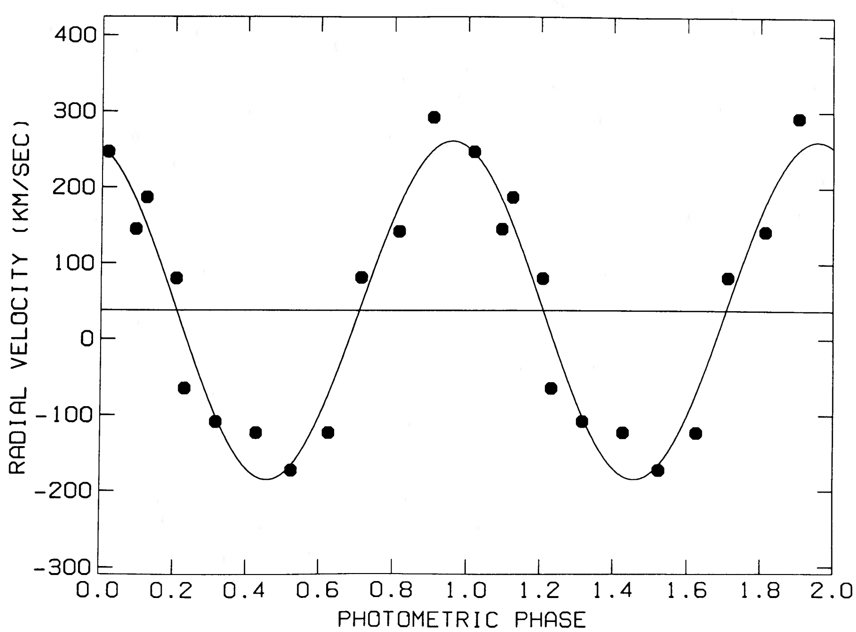

FIG. 10.—The radial velocity curve for the 1985 February 20 Mount Lemmon Hα observations. The measurements were made using a Gaussian width of 300 km s^{-1} and a separation of 2000 km s^{-1}. The amplitude is 223 km s^{-1}.

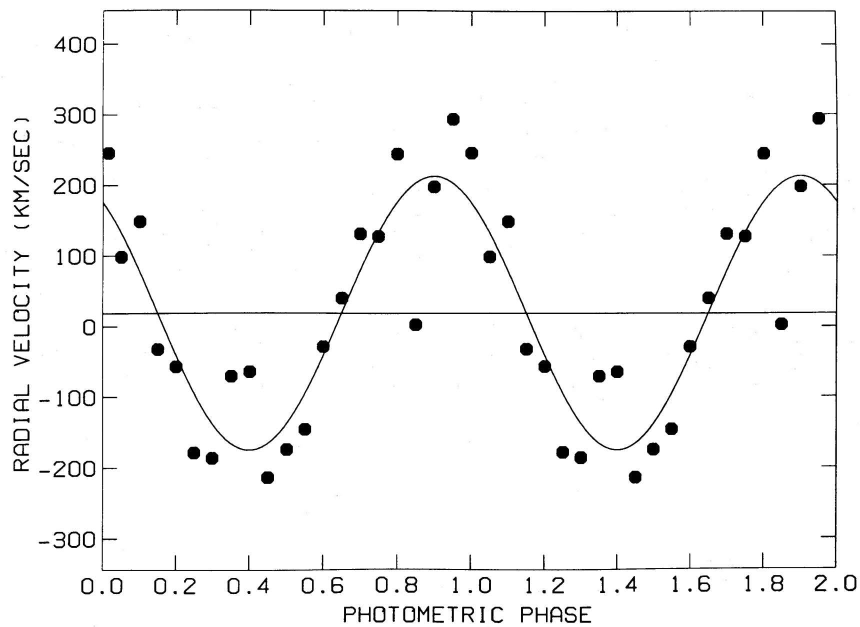

FIG. 11.—The radial velocity curve for the 1984 March McDonald Hβ observations. The spectra were co-added into 20 orbital phase bins prior to measuring the velocities. The velocities are shown folded with the orbital period and plotted as a function of orbital phase. The measurements were made using a Gaussian width of 300 km s^{-1} and a separation of 2400 km s^{-1}. The amplitude is 194 km s^{-1}.

explain the line doubling observed at phase 0.5, then one may wonder why occultation of this extra emission line component by the secondary star does not cause a similar effect. Part of the explanation may be due to the fact that, in addition to the stream and hot spot, a large fraction of the accretion disk is occulted during eclipse. It is therefore unclear whether the eclipse line profile should be expected to resemble the profile observed at phase 0.5. One point appears clear, however, and that is the overall line flux and equivalent width is reduced at phase 0.5 establishing that either absorption of disk emission or occultation of an additional emission component is responsible for the spectral change.

V. CONSTRAINTS ON COMPONENT MASSES

There are several methods available to determine the masses in eclipsing systems. The width of the eclipse alone gives a relationship between the mass ratio and the orbital inclination. Then any two of the following quantities will give the individ-

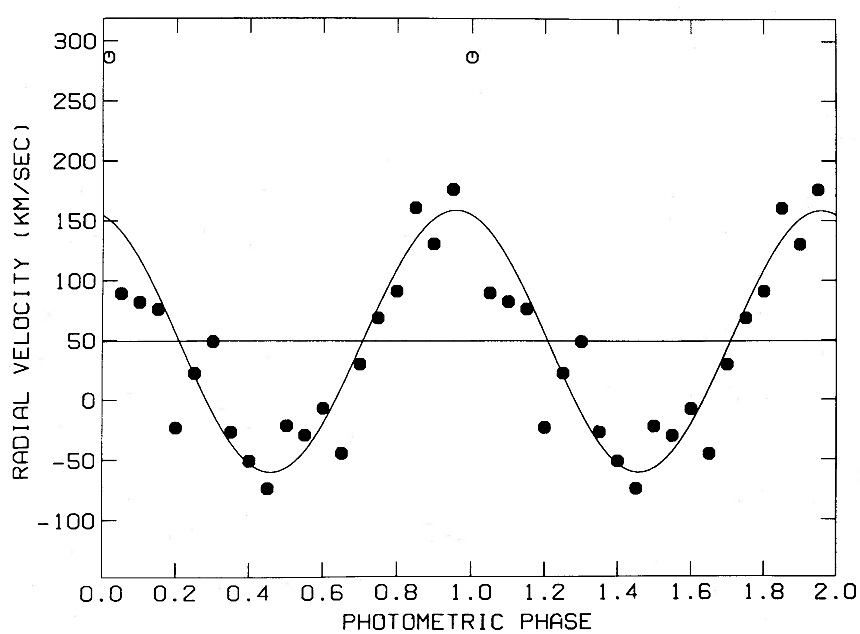

FIG. 12.—The radial velocity curve for the 1984 March McDonald He II λ4686 observations. The measurements were made using a Gaussian width of 300 km s^{-1} and a separation of 2000 km s^{-1}. Because the He II line is strongly affected during eclipse the point at phase 0.0 was given $\frac{1}{2}$ weight in the orbital solution. The amplitude is 109 km s^{-1}.

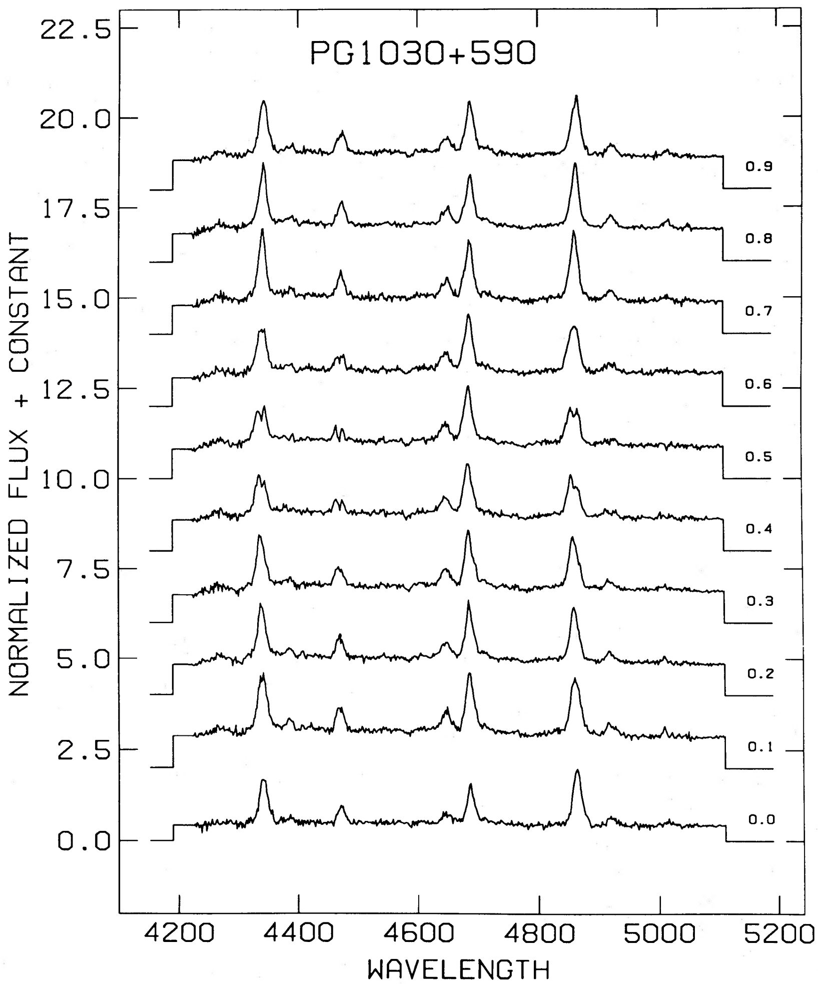

FIG. 13.—The McDonald CCD spectra co-added into 10 orbital phase bins. Note the doubling of the Balmer and He I emission lines near orbital phase 0.5. The diminution of the He II λ4686 emission line strength has already been noted in Fig. 3.

ual masses: (1) the radial velocity amplitude of the white dwarf, K_{wd}; (2) the radial velocity amplitude of the secondary star, K_2; (3) the length of the white dwarf ingress or egress (in conjunction with a suitable mass-radius relation for the white dwarf); (4) a mass-radius relation for the secondary star; (5) the position of the impact point where the mass transfer stream impacts the disk (obtained from the eclipse timing of the hot spot eclipse). It should be pointed out that the hot spot position alone gives a $q-i$ relation and hence only assumption (5) is required to solve for the mass ratio and orbital inclination.

The reliability of the mass determinations depends to some extent on which two assumptions are employed. Unfortunately for some systems not all of the relevant quantities can be measured. For example it is typically the case, as it is for PG 1030+590, that quantities (2), (3), and (5) are not easily determined. For such systems one is forced to use quantities (1) and (4). Specifically, we must assume the radial velocity of the emission lines accurately reflects the motion of the white dwarf and we must adopt a mass-radius relation for the secondary star (usually assumed to be a main-sequence relation). It is unfortunate that the uncertainty inherent in determining quantities (1) and (4) is probably greater than it would be if we could determine any of the other quantities.

Several authors have used the observed eclipse width ($\Delta\Phi$) in conjunction with an estimate of K_{wd} and an assumed mass-radius relation for the secondary star to estimate the component masses in eclipsing cataclysmic variables (e.g., Horne, Lanning, and Gomer 1982; Penning *et al.* 1984; Shafter 1984; Downes *et al.* 1986). Primarily because of the large uncertainty in the value of K_{wd} in PG 1030+590, and to a somewhat lesser extent because of the uncertainty in the exact form of the mass-radius relation for the secondary star, we caution the reader that the masses derived using this procedure are subject to unknown and potentially large systematic errors. However, we feel that it is instructive to explore how the masses depend on a wide range of K-values and on the form of the mass-radius relation for the secondary star.

The procedure adopted here closely parallels that found in Shafter (1984) and the reader is referred to that paper for details of the analysis. Briefly, by adopting a mass-radius relation for the secondary star and noting that the ratio of the secondary star's radius to the stellar separation (R_2/a) is a function only of the mass ratio (Eggleton 1983), it is easy to show that the mass of the secondary is a function of the orbital period and mass ratio only (e.g., see eq. [4], Shafter 1984). For a given value of K_{wd} the mass function of the secondary gives a

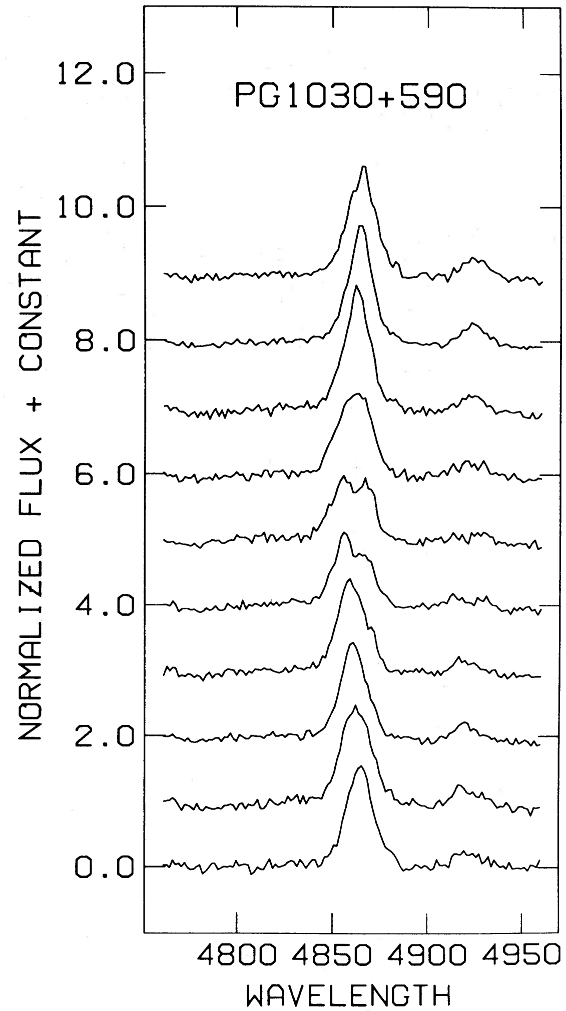

FIG. 14.—The magnified view of the Hβ profile from Fig. 13 showing the line doubling more clearly.

relation between M_2 and the orbital period (P), inclination (i), and mass ratio (q). Assuming that the orbital period is known, these two relations yield a relation between q and i.

An additional relation between q and i may be obtained from the observed eclipse width ($\Delta\Phi$). The eclipse width of PG 1030+590 is somewhat variable, but averaging widths from all of our eclipses we find that $\Delta\Phi = 0.073 \pm 0.003$. For the eclipse of a point source by a spherical body we may write:

$$(R_2/a)^2 = \sin^2(\pi\Delta\Phi) + \cos^2(\pi\Delta\Phi)\cos^2 i\ ,$$

where again R_2/a is a function only of the mass ratio. Here we have approximated the Roche lobe of the secondary as a sphere having the same volume and we have assumed that the continuum emission from the disk is axially symmetric. The $q-i$ relation based on the observed eclipse width is shown in Figure 15. The eclipse width alone places a lower limit of 0.14 on the mass ratio of PG 1030+590.

The two $q-i$ relations form a pair of simultaneous equations with two unknowns which may be solved to yield the orbital inclination and mass ratio. Since the mass of the secondary star is a function of the orbital period and mass ratio, both of which are known, estimates of the individual masses may be computed. The mass-radius relation for the secondary star may be parameterized as follows: $R_2/R_\odot = b(M_2/M_\odot)^x$. Patterson (1984) finds empirically that $b = 1$ and $x = 0.88$ for the lower main sequence. For illustrative purposes we will adopt these values as representative of a main-sequence secondary. For comparison we take $b = 1.5$ and $x = 0.88$ to represent an example of a secondary star which is out of thermal equilibrium and too large for its mass.

The results of our analysis are shown in Figure 16. The white dwarf mass, as determined from the solution of equation (7) of Shafter (1984), is plotted as a function of the secondary star mass for various values of $K_{\rm wd}$ and for two values of the parameter b in the mass-radius relation. As we noted earlier, values of $K_{\rm wd}$ on the order of 200 km s^{-1} or higher imply white dwarf masses less than 0.2 $M_\odot$ and orbital inclinations less than 70°. It is obvious from an inspection of Figure 16 that it is impossible to place useful constraints on the masses without a reliable estimate of $K_{\rm wd}$ and the mass-radius relation of the secondary star. We can make the following observations, however. In general, the mass of the secondary star must be less than $\sim$0.3 $M_\odot$. If we assume that $K_{\rm wd} \gtrsim 100$ km s^{-1} as seems likely, then $M_1 \lesssim 1.0\ M_\odot$ and $i \lesssim 82°$. If the secondary is less dense than a main-sequence star then these upper limits become more severe. Finally, if we cast caution to the wind and assume first that the He II velocities accurately reflect the motion of the white dwarf and second that the secondary is on or near the main sequence then the most probable (or best guess) values for the system parameters are as follows: $M_1 = 0.9\ M_\odot$, $M_2 = 0.29\ M_\odot$, and $i = 80°$.

VI. DISCUSSION

The most surprising result presented in Table 5 is the radial velocity amplitude of the Hα line. The Hα line has an observed amplitude of at least 200 km s^{-1}, which is almost twice the amplitude of He II λ4686. The large discrepancy between the two amplitudes serves to remind us of the danger involved when attempting to infer $K_{\rm wd}$ from radial velocity variations of the emission lines. In addition, although we suspect that the He II emission reflects the motion of the white dwarf more accurately than the Balmer lines, it is hard to imaging how any mechanism could produce the large observed phase shift in the radial velocity curve without affecting the amplitude.

The reliability of using disk emission to infer the motion of the white dwarf in a cataclysmic variable has long been viewed with skepticism. In particular, in some cases like PG 1030+590, it is obvious that the emission line velocity may reflect gas motions which are unrelated to the orbital motion of the white dwarf. Although Downes *et al.* (1986) claim that the measurements of the He II and the Balmer lines in V1315 Aql yield amplitudes which are consistent with each other, a glance at their Figure 10*b* reveals that the amplitude of He II appears to be significantly smaller than the 132 km s^{-1} they derive from Hβ. The situation is similar for PG 1012−035. Honeycutt *et al.* (1986) find an amplitude on the order of 240–280 km s^{-1} for the Balmer lines, but He II λ4686 yields a much smaller value of 170 km s^{-1}. Indeed, in almost every respect PG 1012−035 is remarkably similar to PG 1030+590.

In the final analysis, the only way to assess the reliability of the emission line radial velocities is to obtain an independent measurement of the K-velocity of the white dwarf. The most straightforward technique would involve measuring the velocity of the white dwarf directly. This is usually not possible because the radiation from the white dwarf photosphere is

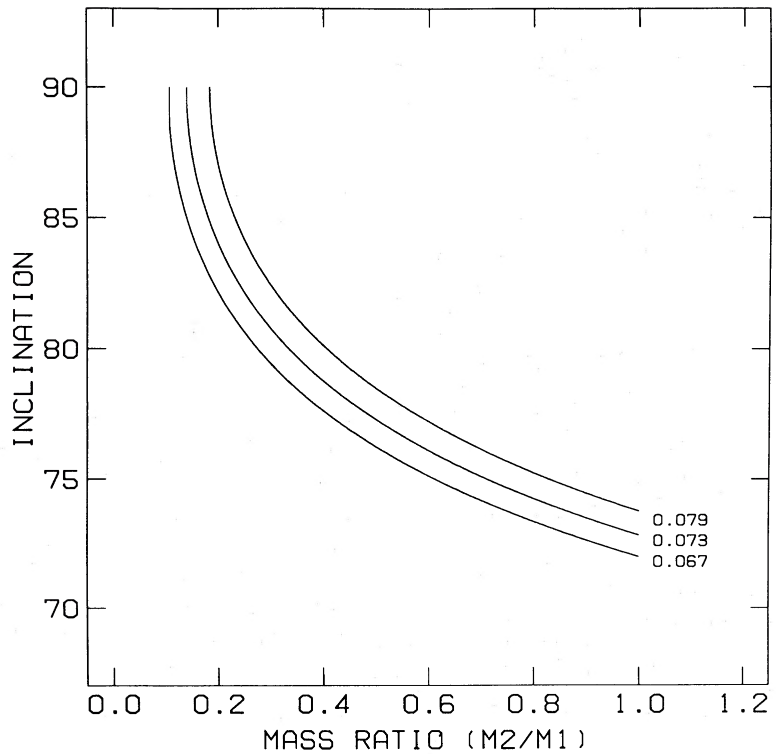

FIG. 15.—The relationship between the mass ratio and the orbital inclination as defined by eq. (2). The orbital inclination is plotted as a function of the mass ratio for three different values of the eclipse width. The mean eclipse width based on our 10 eclipses is 0.073. The other two lines represent $\pm 2\ \sigma$ errors in the measured eclipse width.

drowned out by the disk radiation. There are situations, however, when the mass transfer rate drops precipitously and the underlying spectrum of the white dwarf is revealed. Examples are TT Ari (Shafter *et al.* 1985) and MV Lyr (Robinson *et al.* 1981). Unfortunately in these cases the systems become quite faint ($V \sim 17$ for the two stars mentioned above, making the already difficult radial velocity measurements of the white dwarf even more challenging.

Patterson (1979) has explored the possibility of using the arrival times of the 33 s pulses in AE Aqr to determine the radial velocity amplitude of the white dwarf in this system. Before this technique can be useful the effects of reprocessing of the pulsed light by the outer disk and secondary star must be taken into account. In any case, this technique is obviously restricted to the DQ Her class of magnetic systems.

Hessman *et al.* (1984) measured the radial velocity of the broad Balmer *absorption* lines in the spectrum of SS Cyg during a dwarf nova eruption. Because the physical conditions in the accretion disk during eruption are quite obviously different from the quiescent disk, a measurement of the absorption line radial velocity amplitude should provide an essentially independent estimate of K_{wd}. The results of the Hessman *et al.* study were encouraging in that the absorption line amplitude agreed remarkably well with the emission line amplitude which they measured during quiescence.

To summarize, although obtaining reliable measurements of K_{wd} provides observers with a formidable challenge, the task is not hopeless. As just described, there are potentially a variety of techniques which may be employed to either directly determine K_{wd} or to increase our confidence that the indirect methods are producing reliable estimates of the white dwarf's amplitude.

VII. CONCLUSIONS

We have obtained extensive optical photometry and time-resolved spectroscopy of the cataclysmic variable PG 1030+590. The results of our analysis can be summarized as follows.

1. PG 1030+590 is an eclipsing nova-like variable with a period of 0.1366065 days.

2. The light curve of PG 1030+590 shows no evidence for a "hump" in the light curve prior to eclipse as is seen in many of the eclipsing dwarf novae. There is, however, evidence for a broad hump, centered on eclipse, which shows up in some of our ultraviolet light curves. Overall, the eclipse shape appears to be variable indicating that the disk structure is not stable.

3. Optical spectroscopy of the system revealed the presence of high-excitation emission lines such as He II λ4686, C III λ4650, and C II λ4267. The presence of these features in the spectra of nonmagnetic cataclysmic variables is usually attributed to a high mass accretion rate.

4. Time-resolved spectroscopy revealed the presence of line doubling which occurs near orbital phase 0.5 (when the white dwarf and disk are at inferior conjunction).

5. We have conducted radial velocity studies based on three different emission lines: Hα, Hβ, and He II λ4686. The velocity amplitudes for Hα and Hβ are roughly consistent and yield a value of $K_{em} \approx 200$ km s^{-1}. The higher excitation line, He II λ4686, results in a much lower radial velocity amplitude, $K_{em} = 109$ km s^{-1}. We argue that the He II λ4686 amplitude

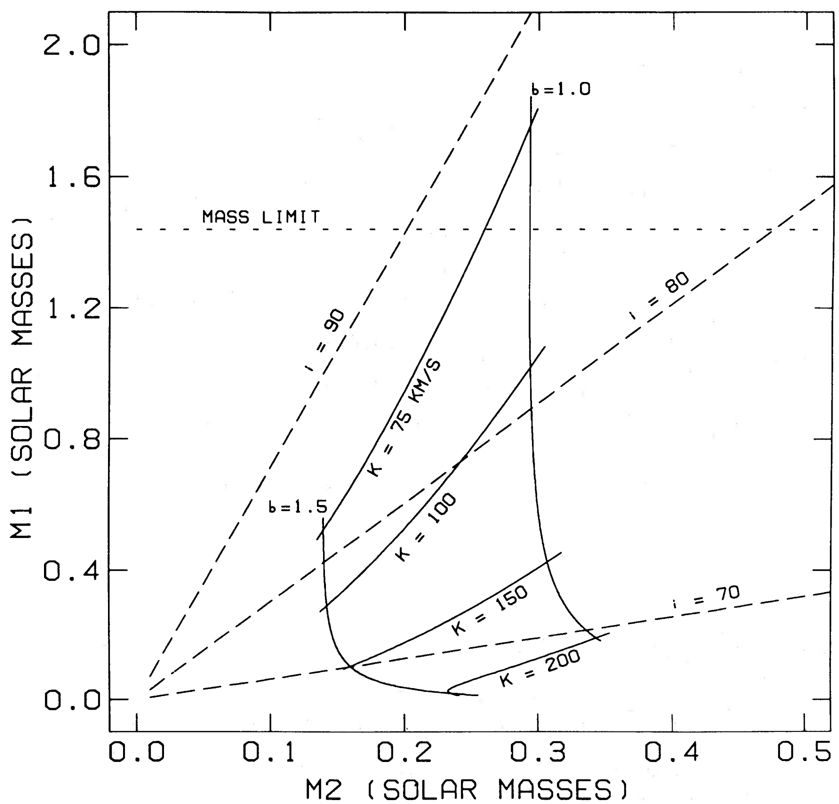

FIG. 16.—Constraints on the component masses are shown based on several representative values of the radial velocity amplitude and the mass-radius relation parameters for the secondary star. Loci of constant orbital inclination (and constant mass ratio) are shown as dashed lines. The horizontal dashed line indicates the Chandrashekhar limit on the mass of the white dwarf. The lines marked with $b = 1$ and $b = 1.5$ represent secondaries having a mean density near the main sequence and less than the main sequence, respectively. If the K-velocity of the white dwarf is 109 km s^{-1} as indicated by the He II emission, and the secondary is near the main sequence then the orbital inclination is near 80° and the masses of the secondary star and the white dwarf are approximately 0.3 and 0.9 $M_{\odot}$, respectively. In any case if K_{wd} is greater than 100 km s^{-1} then the white dwarf mass must be less than a solar mass, while values of K_{wd} above 200 km s^{-1} require the mass of the white dwarf to be below 0.2 $M_{\odot}$.

better reflects the motion of the white dwarf because this line is probably formed in or above the central regions of the accretion disk and as a result would be less affected by hot spot contamination.

6. If we assume that $K_{wd} = K_{em}$(He II) = 109 km s^{-1}, and that the secondary is near the main sequence then the most likely masses are 0.29 $M_{\odot}$ and 0.9 $M_{\odot}$ for the secondary and primary components, respectively. We stress that these values are *highly uncertain.*

7. In general PG 1030+590 appears to be quite similar to PG 1012−035 (Penning *et al.* 1984; Honeycutt, Schlegel, and Kaitchuck 1986) and V1315 Aql (Downes *et al.* 1986). All three systems are eclipsing nova-like variables with orbital periods just above the 2–3 hr period gap, all three systems show a doubling of the low-excitation emission lines near orbital phase 0.5, and all three have radial velocity amplitudes which depend on the excitation of the emission line used in the radial velocity study.

We thank E. L. Robinson and J. H. Wood for their comments on the manuscript, and an anonymous referee for thoughtful comments. This research has been supported in part by NSF grant AST85-00790. A. W. S. and F. V. H. acknowledge the generous allotment of observing time made available at the Mount Lemmon Observatory.

REFERENCES

Cook, M., and Warner, B. 1984, *M.N.R.A.S.*, **207**, 705.
Cordova, F. A., and Mason, K. O. 1983, in *Accretion Driven Stellar X-Ray Sources*, ed. W. H. G. Lewin and E. P. J. van den Heuvel (Cambridge: Cambridge University Press), p. 147.
Downes, R. A., Mateo, M., Szkody, P., Jenner, D. C., Margon, B. 1986, *Ap. J.*, **301**, 240.
Eggleton, P. P. 1983, *Ap. J.*, **268**, 368.
Gilliland, R. L., Kemper, E., and Suntzeff, N. 1986, *Ap. J.*, **301**, 252.
Green, R. F., Ferguson, D. H., and Liebert, J. 1982, *Pub. A.S.P.*, **94**, 560.
Hessman, F. V. 1986, *Ap. J.*, **300**, 794.
Hessman, F. V., Robinson, E. L., Nather, R. E., and Zhang, E. H. 1984, *Ap. J.*, **286**, 747.
Honeycutt, R. K., Kaitchuck, R. H., and Schlegel, E. M. 1987, *Ap. J. Suppl.*, **65**, 451.
Honeycutt, R. K., Schlegel, E. M., and Kaitchuck, R. H. 1986, *Ap. J.*, **302**, 388.
Horne, K. 1985, *M.N.R.A.S.*, **213**, 129.
Horne, K., Lanning, H. H., and Gomer, R. H. 1982, *Ap. J.*, **252**, 681.
Kaitchuck, R. H., Honeycutt, K., and Schlegel, E. M. 1983, *Ap. J.*, **267**, 239.
Marsh, T. R., Horne, K., and Shipman, H. L. *M.N.R.A.S.*, **225**, 551.
Moffat, T. J., and Barnes, T. G. 1979, *A.J.*, **84**, 627.
Nather, R. E. 1973, *Vistas Astr.*, **15**, 91.
Patterson, J. 1979, *Ap. J.*, **234**, 978.
———. 1984, *Ap. J. Suppl.*, **54**, 443.
Penning, R. W., Ferguson, D. H., McGraw, J. T., Liebert, J., and Green, R. F. 1984, *Ap. J.*, **276**, 233.
Rappaport, S., Verbunt, F., and Joss, P. C. 1983, *Ap. J.*, **275**, 713.
Robinson, E. L. 1976, *Ann. Rev. Astr. Ap.*, **14**, 119.
Robinson, E. L., Barker, E. S., Cochran, A. L., Cochran, W. D., and Nather, R. E. 1981, *Ap. J.*, **251**, 611.
Robinson, L. B., and Wampler, E. J. 1972, *Pub. A.S.P.*, **84**, 161.

Schlegel, E. M., Honeycutt, R. K., and Kaitchuck, R. H. 1983, *Ap. J. Suppl.*, **53**, 397.
Schneider, D. P., and Young, P. J. 1980, *Ap. J.*, **238**, 946.
Schneider, D. P., Young, P., and Shectman, S. A. 1981, *Ap. J.*, **245**, 644.
Shafter, A. W. 1984, *A.J.*, **89**, 1555.
———. 1985, in *Cataclysmic Variables and Low Mass X-ray Binaries*, ed. D. Q. Lamb and J. Patterson (Dordrecht: Reidel), p. 355.
Shafter, A. W., and Harkness, R. P. 1986, *A.J.*, **92**, 658.
Shafter, A. W., and Hessman, F. V. 1984, *Bull. AAS*, **16**, 505.
Shafter, A. W., Szkody, P., Liebert, J., Penning, W. R., and Bond, H. E. 1985, *Ap. J.*, **290**, 707.
Shafter, A. W., Szkody, P., and Thorstensen, J. R. 1986, *Ap. J.*, **308**, 765.
Shafter, A. W., Wheeler, J. C., and Cannizzo, J. K. 1986, *Ap. J.*, **305**, 261.
Shafter, A. W., Wood, J. H., and Robinson, E. L. 1988, (Paper II) in preparation.
Smak, J. 1971, *Acta Astr.*, **21**, 15.
———. 1984, *Acta Astr.*, **34**, 161.
Stone, R. P. S. 1977, *Ap. J.*, **218**, 767.
Stover, R. J. 1981, *Ap. J.*, **249**, 673.
Wade, R. A., and Ward, M. J. 1985, in *Interacting Binary Stars*, ed. J. E. Pringle and R. A. Wade (Cambridge: Cambridge University Press), p. 129.
Warner, B. 1976, in *IAU Symposium 73, The Structure and Evolution of Close Binaries*, ed. P. Eggleton, S. Mitton, and J. Whelan (Dordrecht: Reidel), p. 85.
Warner, B., and Nather, R. E. 1971, *M.N.R.A.S.*, **152**, 219.
Wood, J. H., Horne, K., Berriman, G., Wade, R. A., O'Donoghue, D., and Warner, B. 1986, *M.N.R.A.S.*, **219**, 629.
Young, P., Schneider, D. P., and Shectman, S. A. 1981, *Ap. J.*, **245**, 1035.
Zhang, E.-H., Robinson, E. L., and Nather, R. E. 1986, *Ap. J.*, **305**, 740.

F. V. HESSMAN: Max-Plank-Institut für Astronomie, 6900 Heidelberg/Königstuhl, FRG

A. W. SHAFTER: Department of Astronomy, University of Texas, Austin, TX 78712

E.-H. ZHANG: Beijing Astronomical Observatory, Chinese Academy of Sciences, Beijing, 100080 China